Supporting Information

Insights into the mechanism of enhanced methane low-temperature coupling conversion over the zeolite-encaged Ni-Pt catalysts

Lunan Wu[a], Xiu-Jie Yang[a,*], Jun Li[b], Weichao Chou[c], Bin Lou[a,*], Jing Wu[d], Nan Shi[a], Fushan Wen[a], Dong Liu [a,*]

[a] *State Key Laboratory of Heavy Oil Processing, China University of Petroleum, Qingdao, Shandong 266580, China*

[b] *CNOOC Institute of Chemicals & Advanced Materials, Beijing 102200, China*

[c] *Dalian Institute of Chemical Physics, Chinese Academy of Sciences, Dalian 116023, China*

[d] *PetroChina Liaohe Petrochemical Company, Panjin, Liaoning, 124000, China*

∗ Corresponding authors.

E-mail Address: yangxiujie@upc.edu.cn (X. Yang), louloulove@163.com (B. Lou), liudong@upc.edu.cn (D. Liu)

Experimental Section

Chemicals

Chloroplatinic acid hexahydrate ($H_2PtCl_6 \cdot 6H_2O$, ~37.5 wt% Pt), colloidal silica (30 wt% in water), aluminum sulfate octadecahydrate ($A1_2(SO_4)_3 \cdot 18H_2O$), ammonium chloride ($NH_4Cl$, 99.8%) and n-hexane ($C_6H_{14}$, 99%) were purchased from Macklin Biochemical Technology Ltd. Sodium hydroxide (NaOH, 99%), nickel nitrate hexahydrate ($Ni(NO_3)_2 \cdot 6H_2O$, 98%), ethanediamine (EDA, 99%) and tetrapropylammonium hydroxide solution (TPAOH, 25 wt% in water) were obtained from Sinopharm Chemical Reagent Ltd. All the chemical reagents were used without any further treatment.

Characterization

X-ray diffraction (XRD) was detected using a Bruker D8 Advance X-ray diffractometer. Scanning electron microscope (SEM) images were recorded on a ZEISS MERLIN microscope. High-resolution transmission electron microscopy (HRTEM) and high-angle annular dark-field scanning transmission electron microscope (HAADF-STEM) images were taken on a Thermo

Scientific Talos F200X microscope. X-ray photoelectron spectroscopy (XPS) was measured on a Thermo Scientific K-alpha 250Xi spectrometer. Inductively coupled plasma-optical emission spectroscopy (ICP-OES) was tested on a Agilent 720ES spectrometer to analyze the chemical components of samples. The specific surface area, pore diameter and pore volumes of samples were calculated from nitrogen adsorption-desorption isotherms recorded on a ASAP 2020 micropore system. Hydrogen temperature programmed reduction (H_2-TPR), methane temperature programmed reaction (CH_4-TPR) and temperature-programmed desorption of ammonia (NH_3-TPD) were acquired on a Micromeritics AutoChem II 2920 chemisorption analyzer. Temperature-programmed desorption of methane (CH_4-TPD) was conducted on a VDsorb-91i chemisorption analyzer. The ^{29}Si and ^{27}Al MAS NMR spectra of zeolite samples were performed on a Bruker Advance III 500 MHz spectrometer at 59.57 and 78.13 MHz, respectively. CO pulse adsorption was conducted on a ChemStar automated chemisorption analyzer to ascertain the dispersity of metals on the zeolite. The UV–vis diffuse reflectance spectra (UV-vis DRS) of zeolites were recorded on a Shimadzu UV-2700 ultraviolet-visible spectrophotometer in the range of 200-800 nm. Thermal gravimetric analyses (TGA)of spent catalysts were performed on a STA 449 F5 simultaneous thermal analyzer from 25 to 800 ℃ in air. Raman spectra were conducted using a Thermo Scientific DXR Raman spectrometer.

Fourier transform infrared (FT-IR) spectra of pyridine adsorption were conducted on a Bruker Tensor 27 infrared spectrometer. The samples were degassed at 300 ℃ for 1 h under vacuum condition. Next, pyridine was injected into reaction tank for 30min after cooled to room temperature and then heated to 100 ℃, respectively. FT-IR spectra of pyridine adsorption were recorded in the range 400-4000 cm^{-1}. CO-diffuse reflectance infrared fourier transform spectra (CO-DRIFTS) were analyzed using a Nicolet iS50 infrared spectrometer. Typically, the catalysts were reduced in a flow of H_2 (25 mL/min) at 300 ℃ for 1 h. and then cooled to 25 ℃ in pure He (40 mL/min). Next, 5%CO/He (50 mL/min) was introduced into the cell for 30 min. The spectra were recorded at the set time after scavenging with pure He (30 mL/min).

The electrochemical impedance spectra of the catalyst were carried out using the CHI 660E electrochemical workstation. The Pt electrode and the saturated Ag/AgCl electrode were used as counter electrode and reference electrode. The preparation method of the working electrode is as follows: Firstly, 10 mg catalysts, ethanol and 50 μL 0.5% Nafion solution are

mixed together and ultrasonic for 30 min. Then, the mixture is evenly spread on the ITO glass and dried at 60 ℃ to prepare the working electrode. The electrolyte solution was 0.2 M Na_2SO_4 aqueous solution. Electrochemical impedance spectra were tested with the frequency range of 10000~ 0.01 Hz.

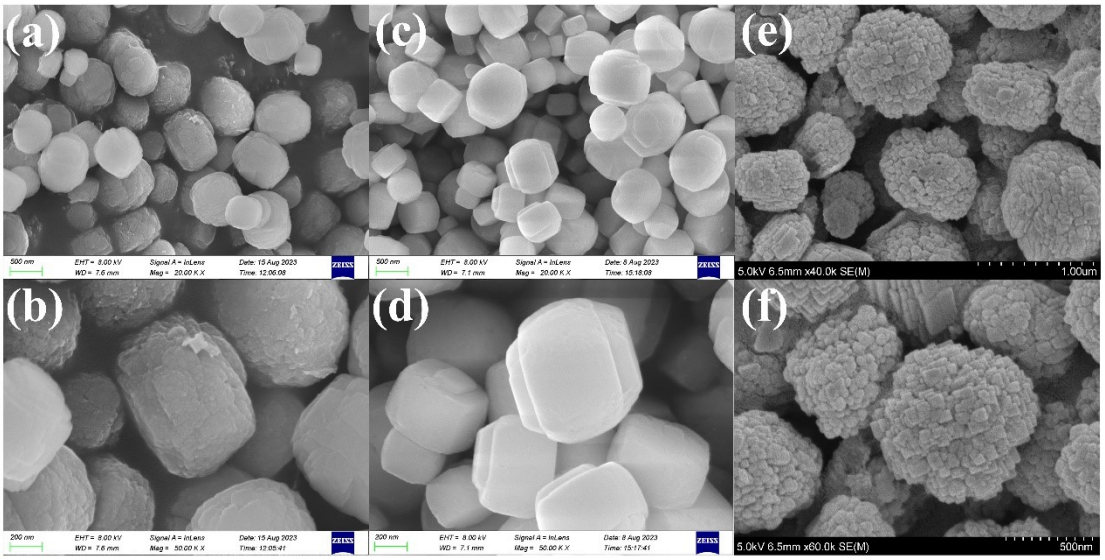

Fig. S1 SEM images of (a-b)Ni-Pt@ZSM-5(100), (c-d)Ni-Pt@S-1 and (e-f)Ni-Pt/ZSM-5(25).

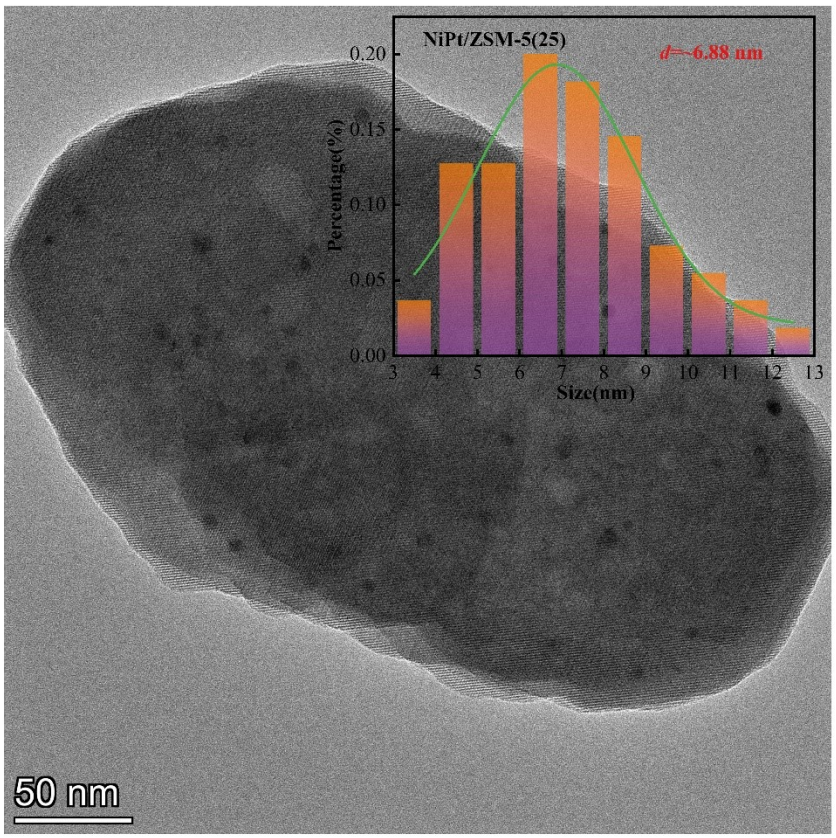

Fig. S2 HRTEM image of Ni-Pt/ZSM-5(25).

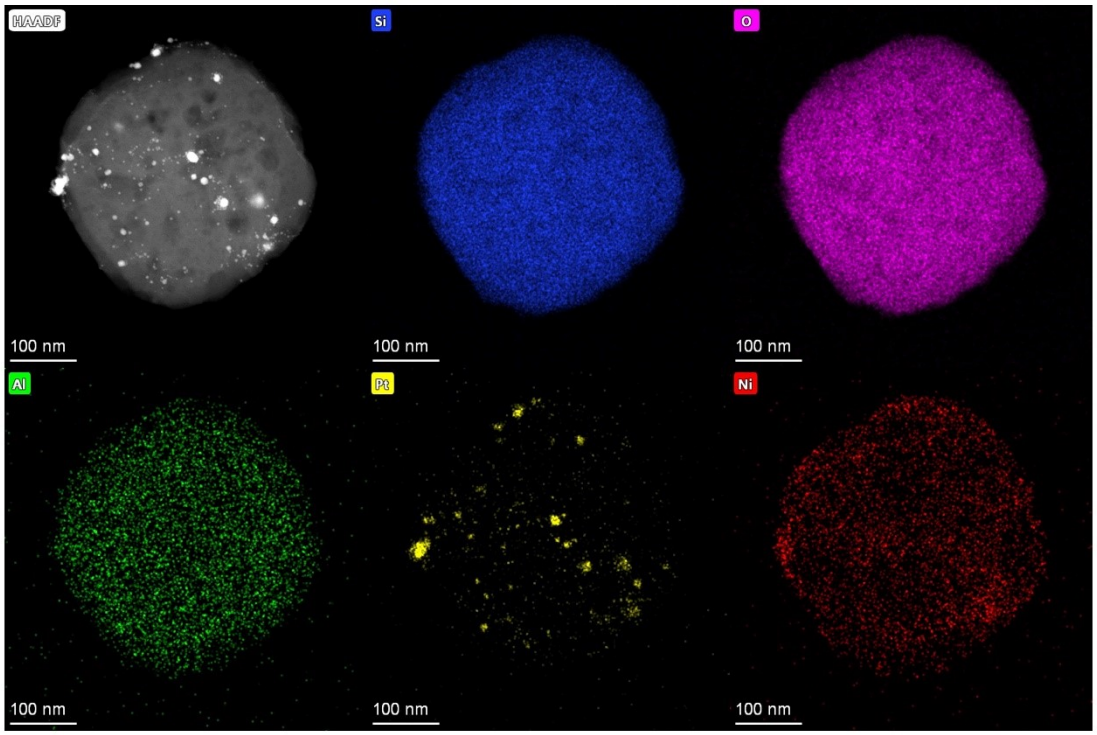

Fig. S3 STEM images of Ni-Pt/ZSM-5(25).

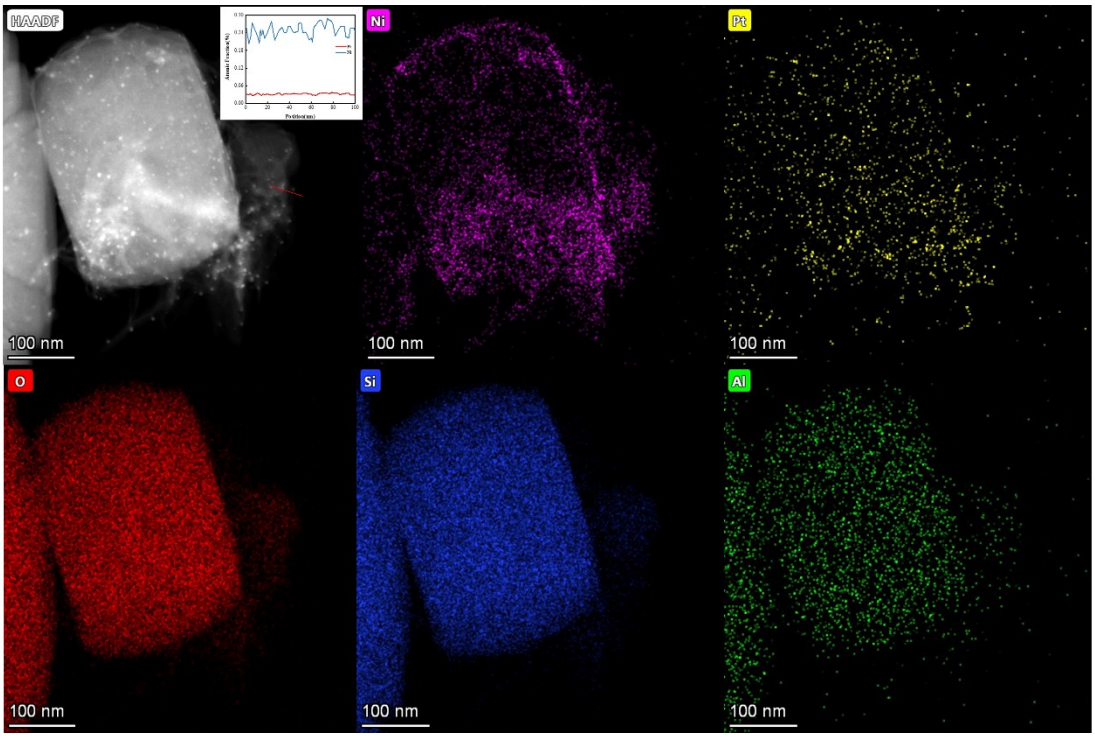

Fig. S4 Tomographic STEM images and line-scan EDS of Ni-Pt@ZSM-5(25).

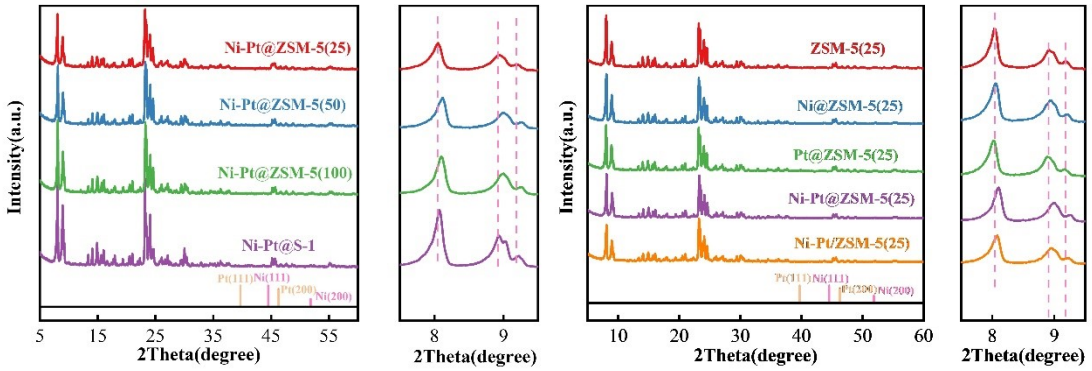

Fig. S5 XRD patterns of as-prepared catalysts.

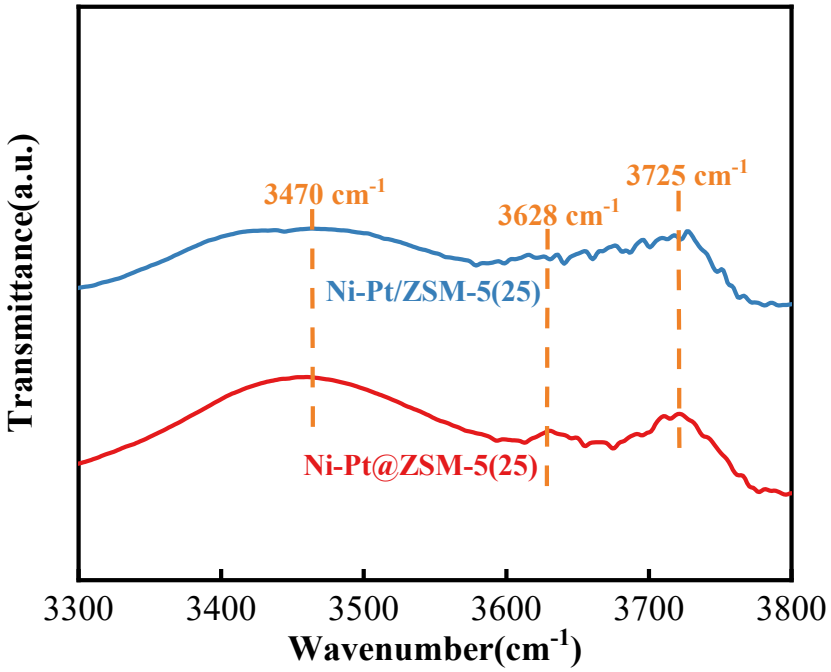

Fig. S6 IR spectra of OH stretching vibrations region

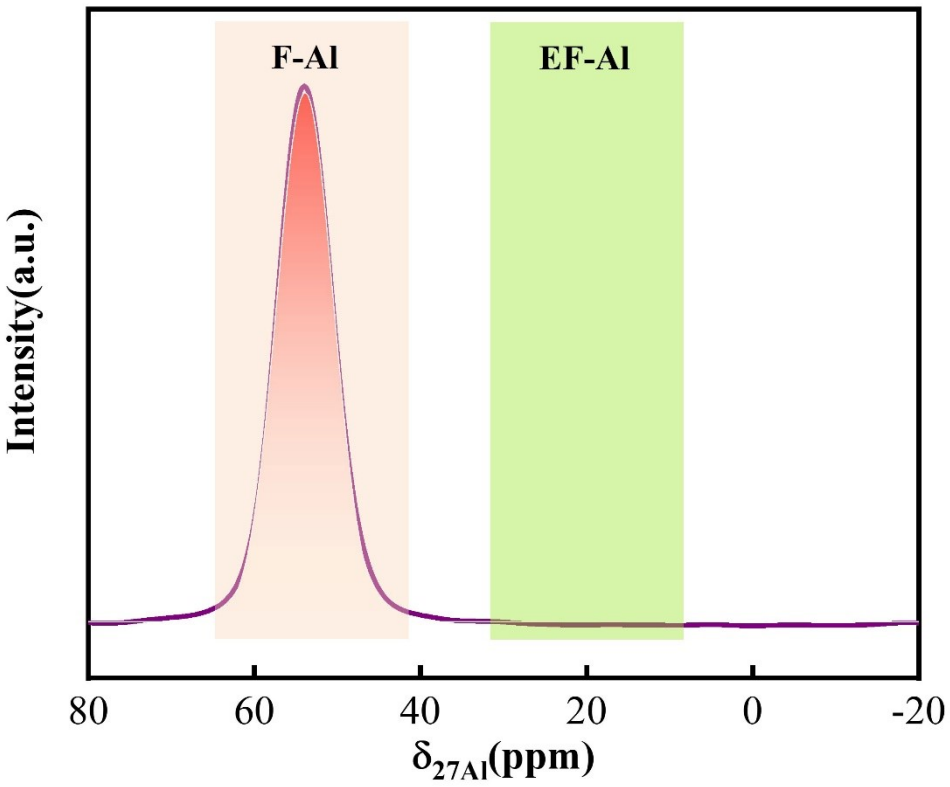

Fig. S7 ^{27}Al MAS NMR spectrum of Ni-Pt@ZSM-5(25)

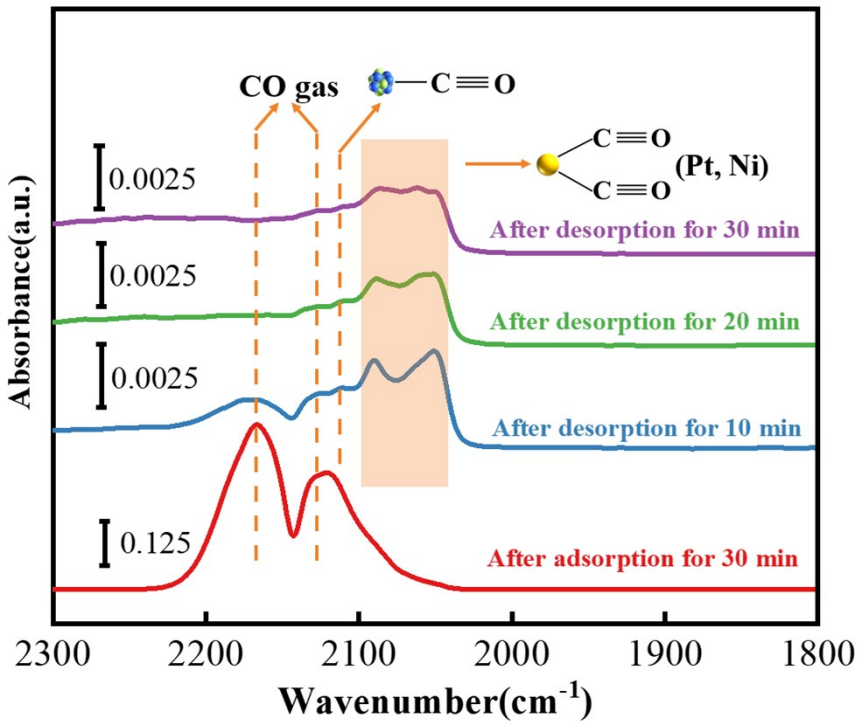

Fig. S8 CO-diffuse reflectance infrared Fourier transform spectra of Ni-Pt/ZSM-5(25).

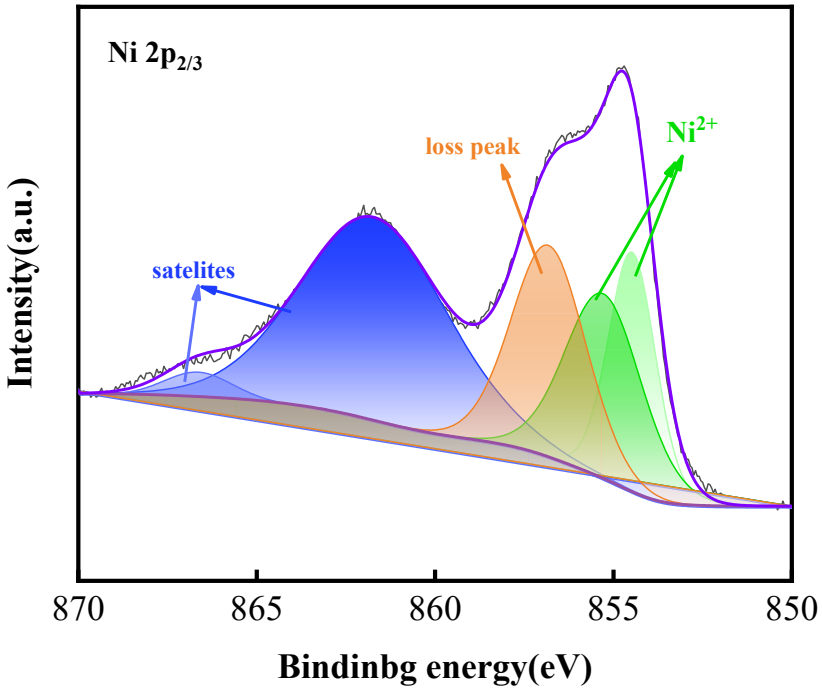

Fig. S9 Ni $2p_{2/3}$ spectrum of NiO.

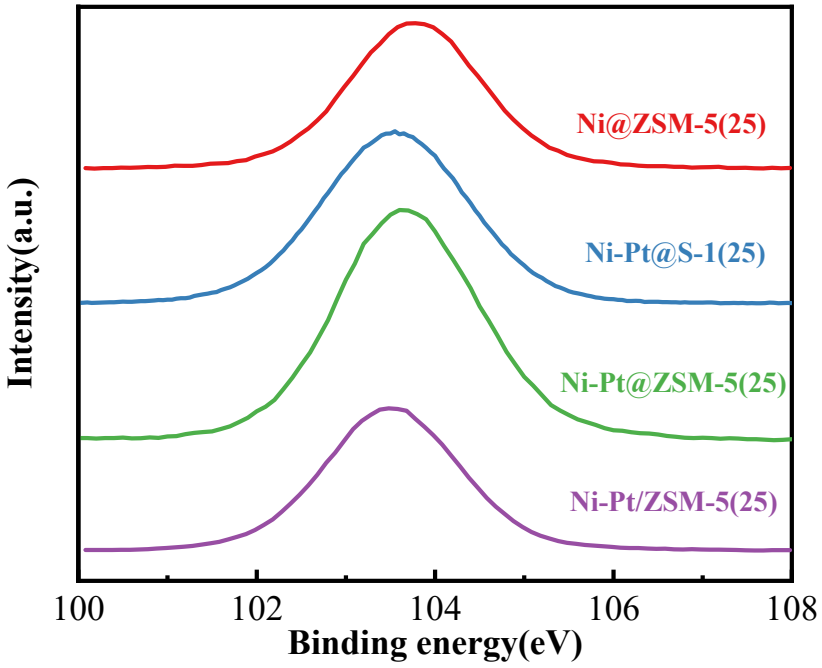

Fig. S10 Si 2p spectra of as-prepared catalysts.

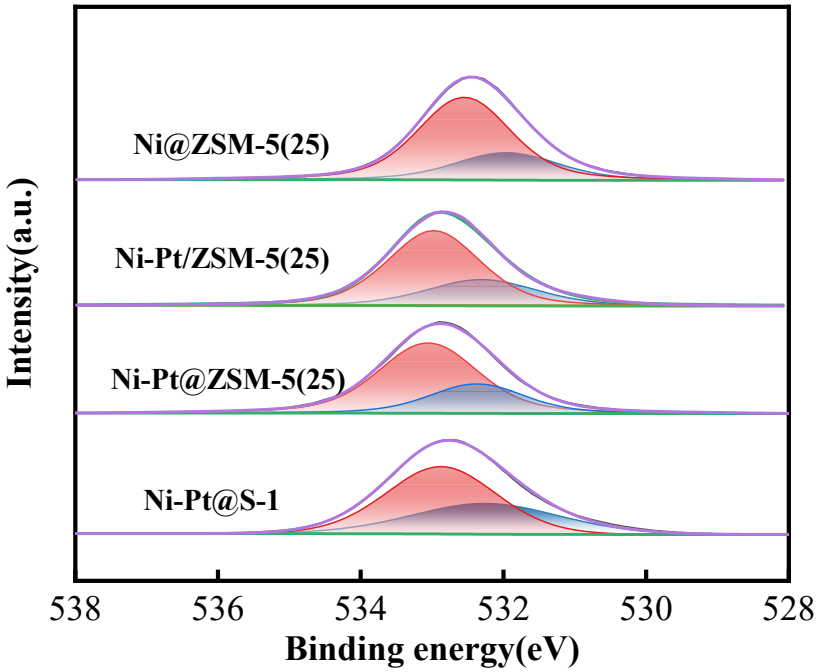

Fig. S11 O 1s spectra of as-prepared catalysts.

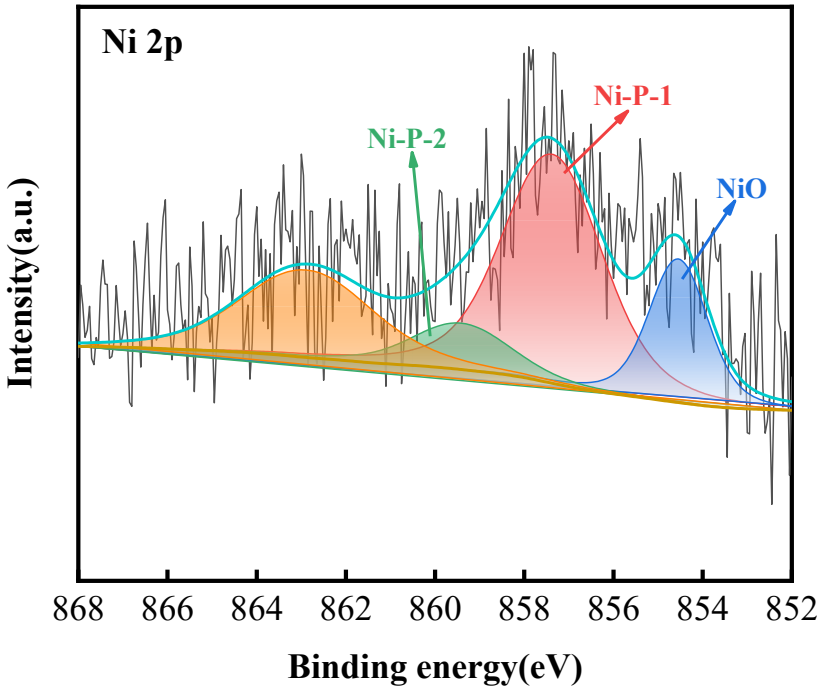

Fig. S12 (a) Ni 2p spectra of Ni-Pt@ZSM-5(25) without reduction.

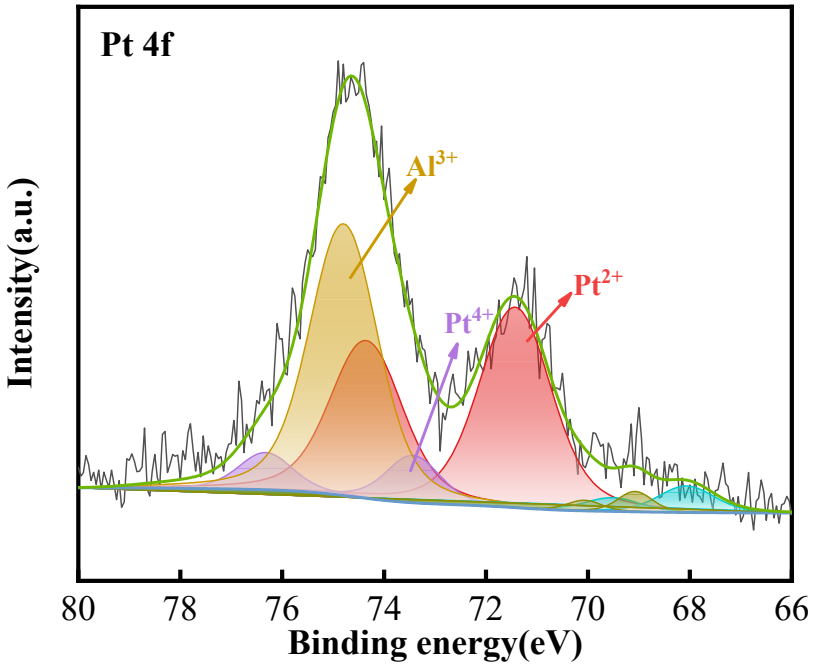

Fig. S13 Pt 4f spectrum of Ni-Pt@ZSM-5(25) without reduction.

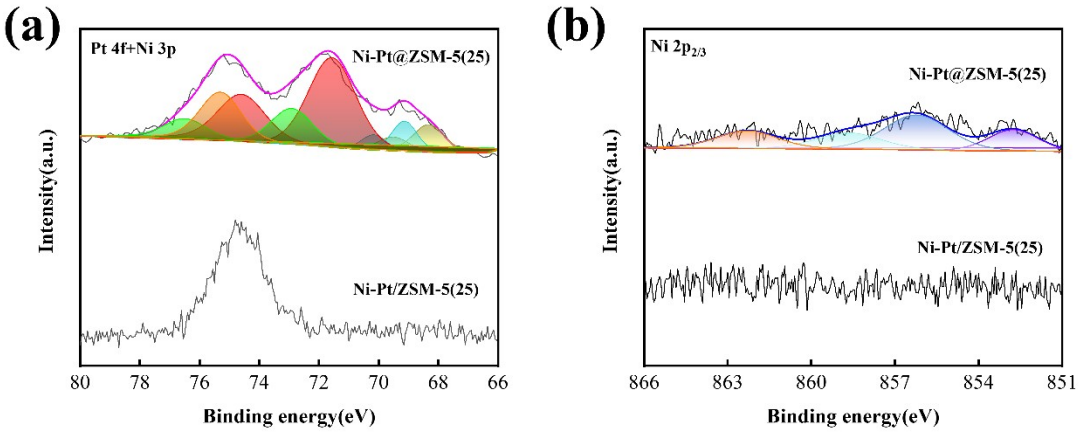

Fig. S14 (a) Ni 2p and (b) Pt 4f spectra of Ni-Pt@ZSM-5(25) and Ni-Pt/ZSM-5 after depth profiling.

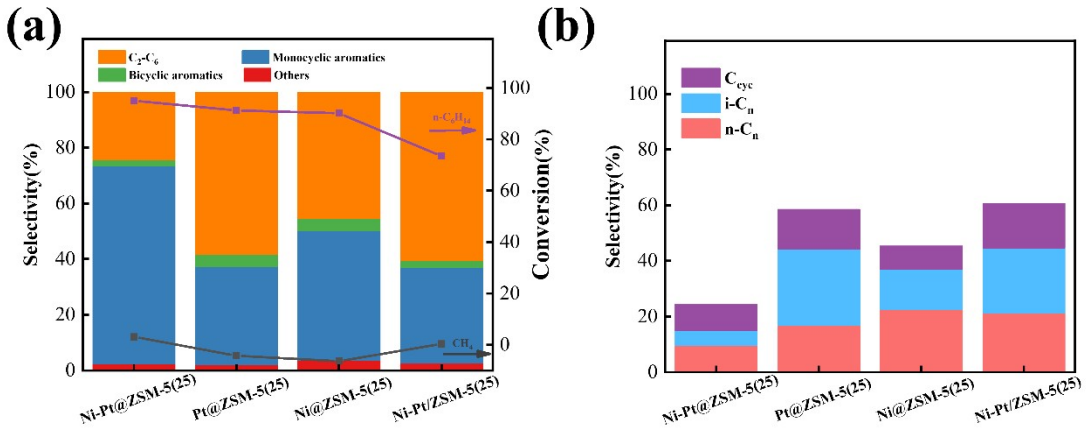

Fig. S15 The co-aromatization performance of different catalysts at 400 °C. (a) The conversion of *n*-hexane and the detailed selectivity of C_1-C_6; (b) The selectivity of gas products. (Reaction conditions：*m*(Catalysts)=0.2 g; *p*＝1.0 MPa; *m*(*n*-hexane)=15 g; *t*=60 min； *T*=400 °C; C_{cyc}——cycloalkanes; n-C_n——n-alkanes; n-C_n——iso- alkanes)

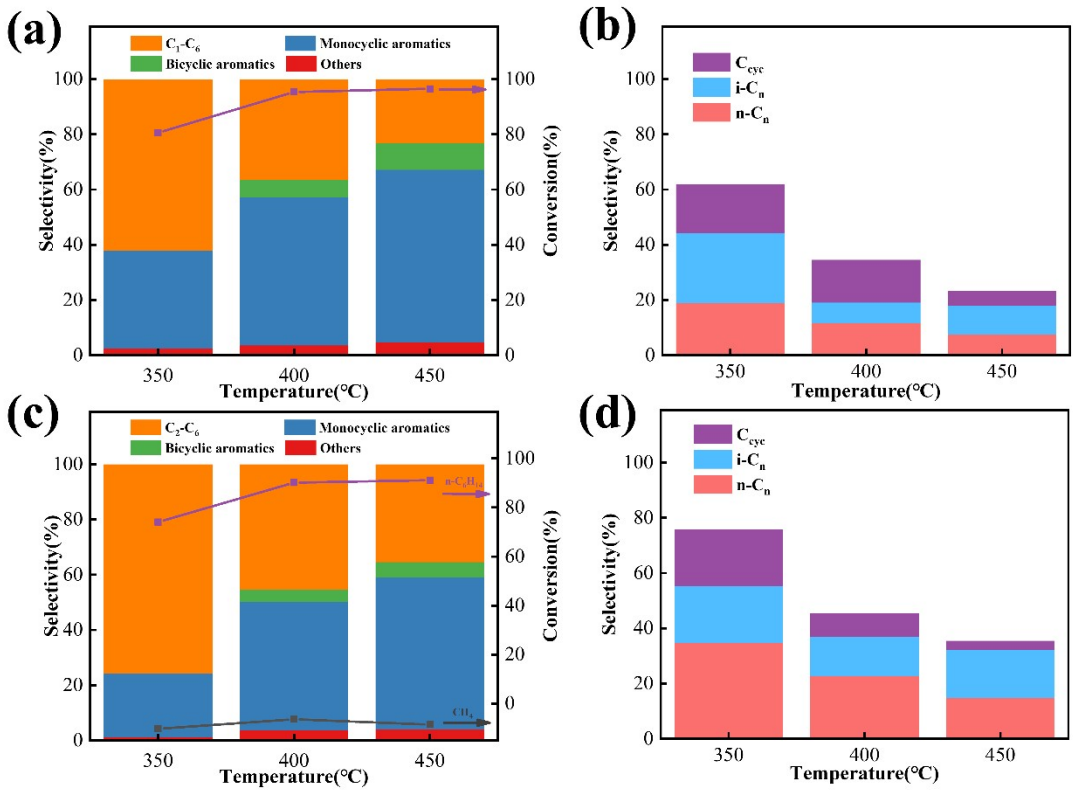

Fig. S16 The conversion of *n*-hexane, the selectivity of total products and the detailed selectivity of C_1-C_6 in the aromatization of *n*-hexane over Ni@ZSM-5(25) at different

temperature under different environment. (a-b) Nitrogen; (c-d) Methane. (Reaction conditions：*m*(Catalysts)=0.2 g; *p*＝1.0 MPa; *m*(*n*-hexane)=15 g; *t*=60 min; C_{cyc}——cycloalkanes; n-C_n——n-alkanes; n-C_n——iso- alkanes)

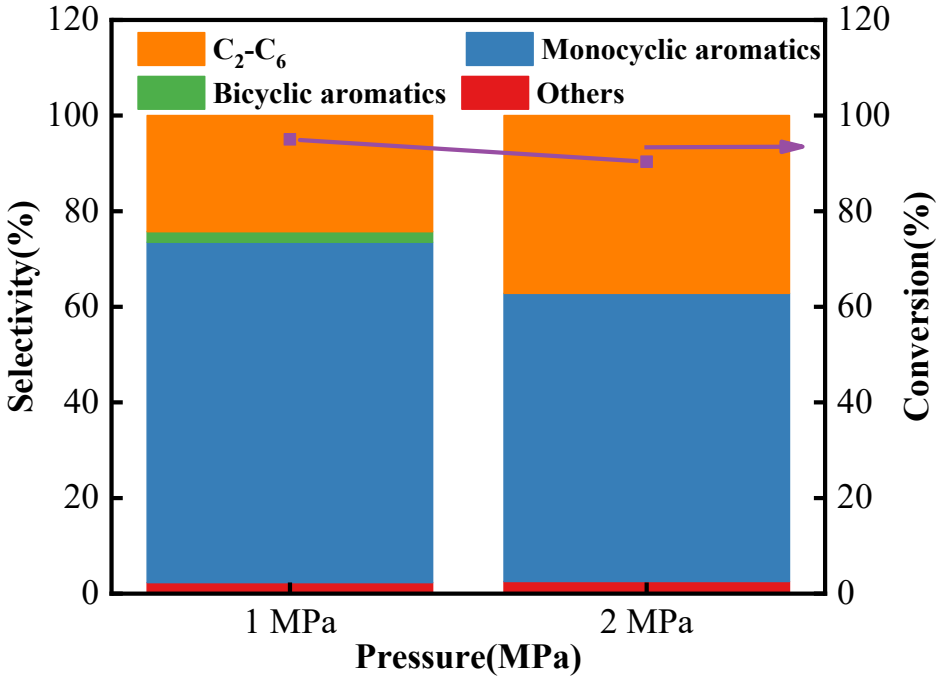

Fig. S17 The conversion of n-hexane and the selectivity of total products in the aromatization of n-hexane over Ni-Pt@ZSM-5(25) under different pressure. (Reaction conditions：*m*(Catalysts)=0.2 g; *p*＝1.0 MPa; *m*(*n*-hexane)=15 g; *t*=60 min； *T*=400 ℃; C_{cyc}——

cycloalkanes; n-C_n——n-alkanes; n-C_n——iso- alkanes)

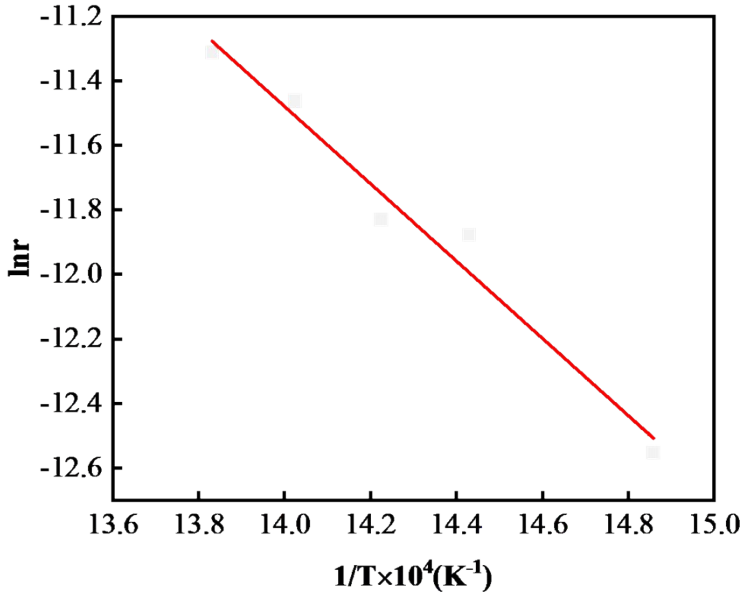

Fig. S18. Arrhenius plots of lnr vs. 1/T for methane over Ni-Pt@ZSM-5 (25).

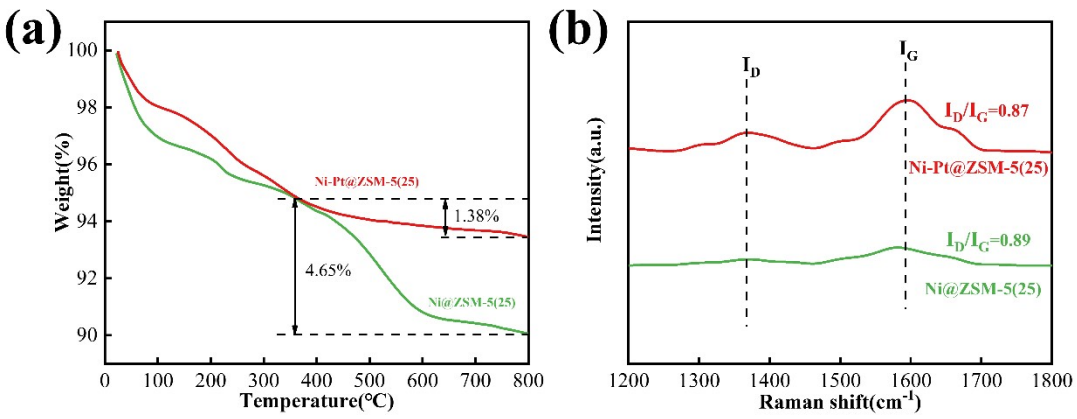

Fig. S19 (a)TG profiles and (b) Raman spectra of spent catalysts in the co-aromatization

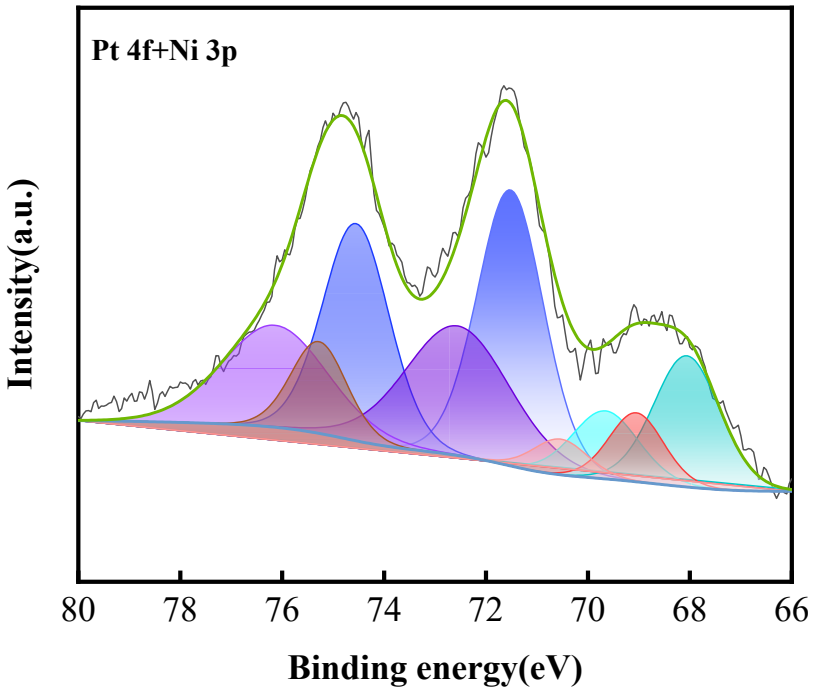

Fig. S20 Pt 4f spectrum of the spent Ni-Pt@ZSM-5(25).

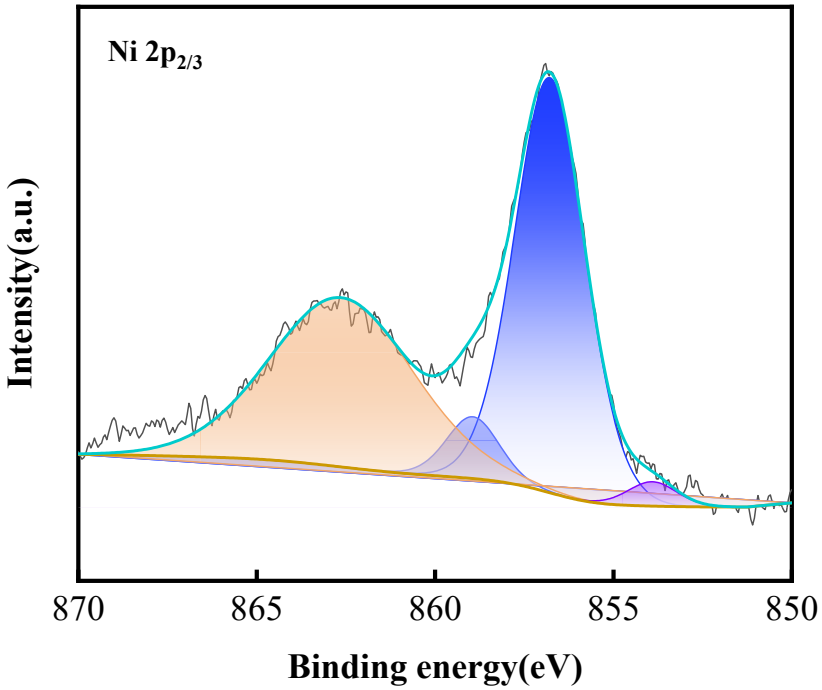

Fig. S21 Ni 2p spectrum of the spent Ni-Pt@ZSM-5(25).

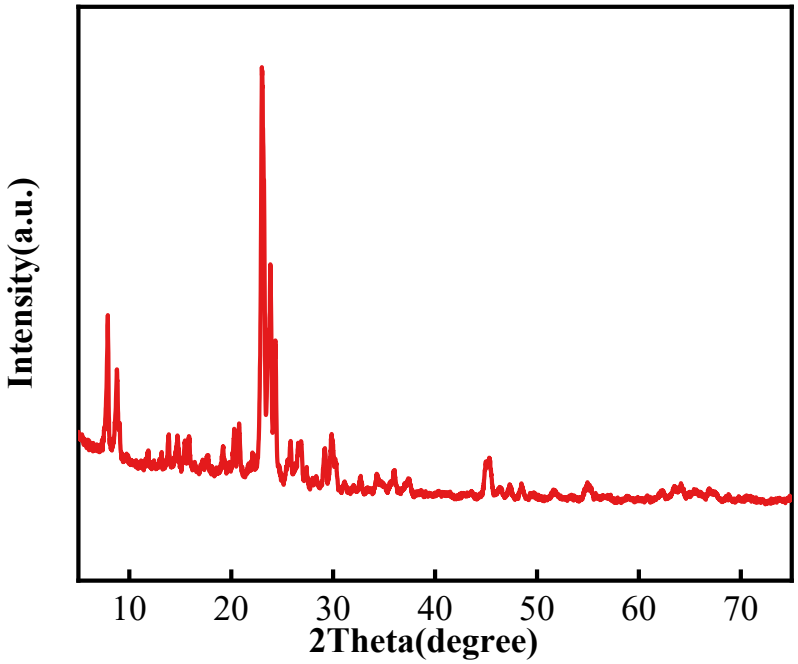

Fig. S22 XRD of the spent Ni-Pt@ZSM-5(25).

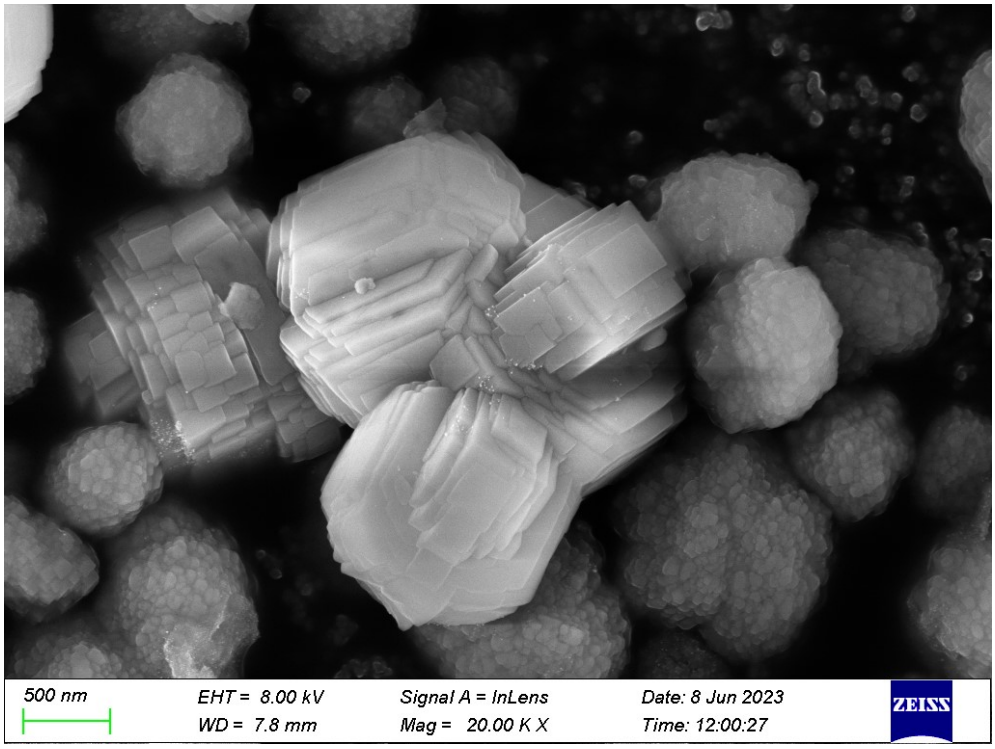

Fig. S23 SEM of the spent Ni-Pt@ZSM-5(25).

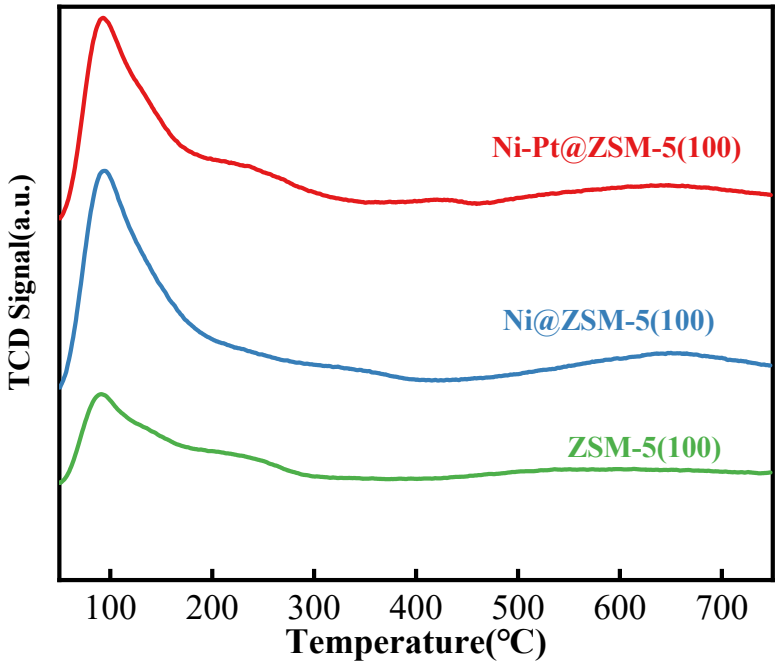

Fig. S24 NH_3-TPD of as-prepared catalysts.

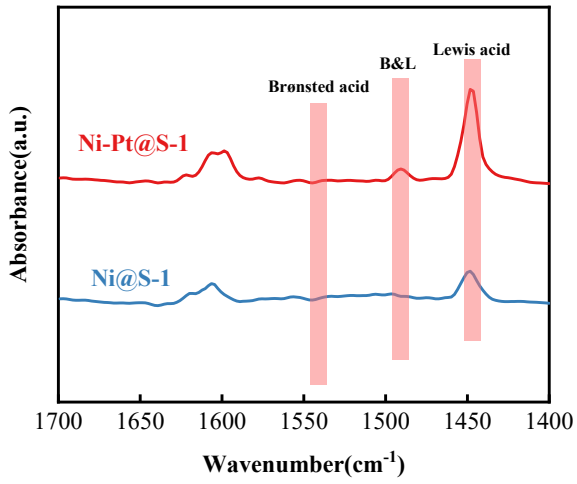

Fig. 25 FT-IR spectra of pyridine adsorption of Ni-Pt@S-1 and Ni@S-1.

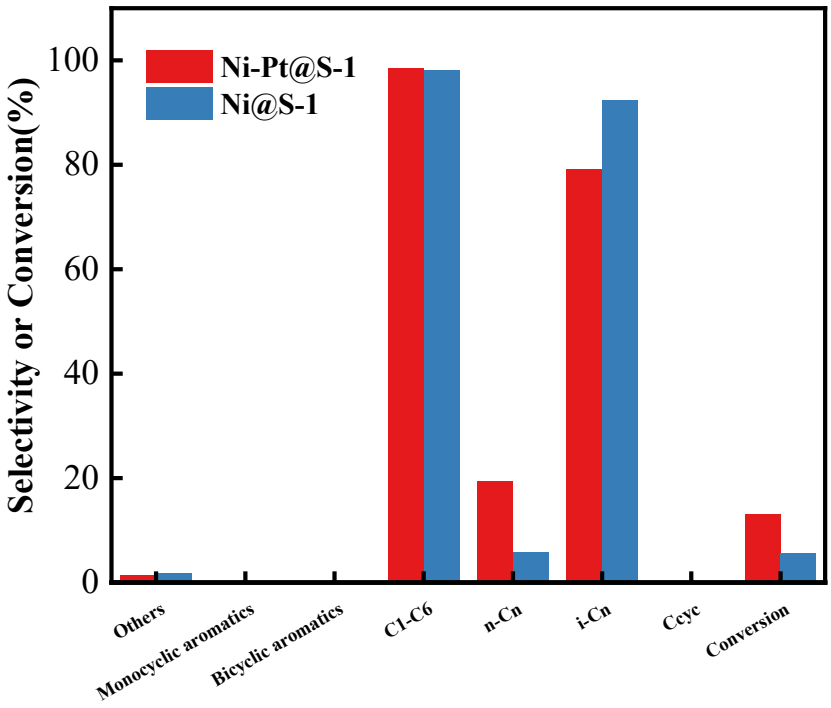

Fig. S26 The aromatization of *n*-hexane performance of Ni-Pt@S-1 and Ni@S-1.

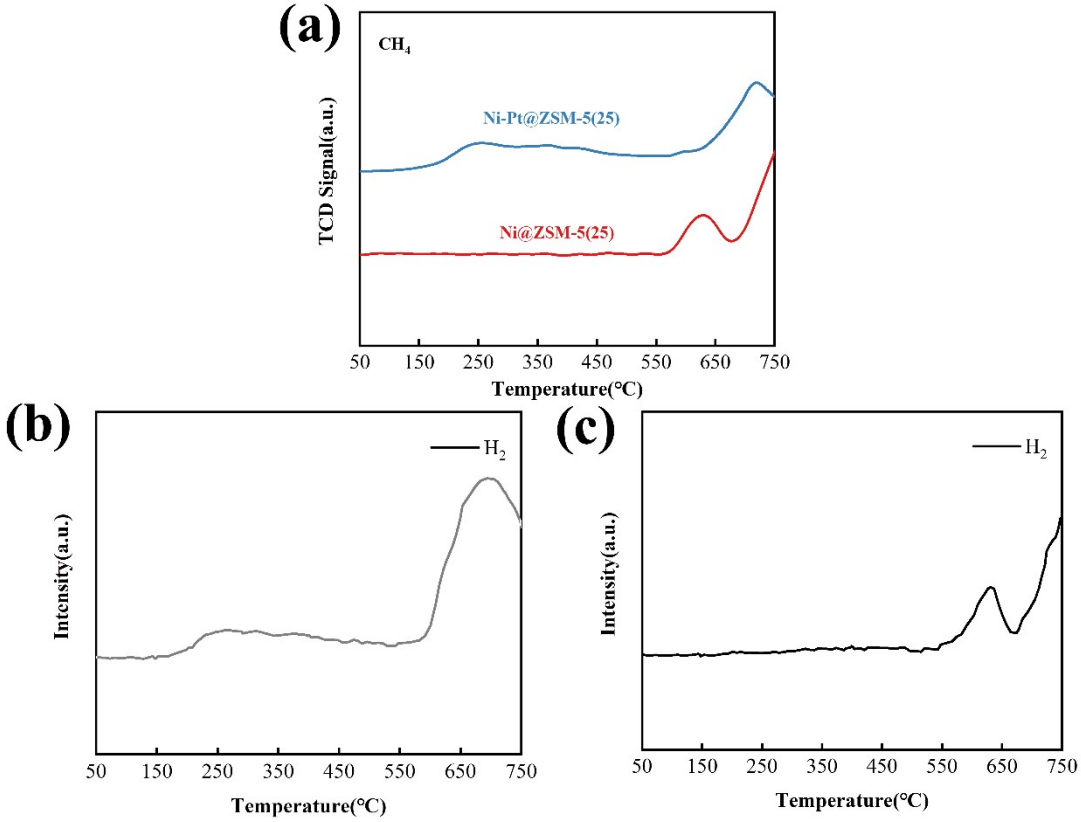

Fig. S27 (a) CH_4 signals on the catalysts during TPSR and H_2 signals on Ni-Pt@ZSM-5(25) and Ni@ZSM-5(25).

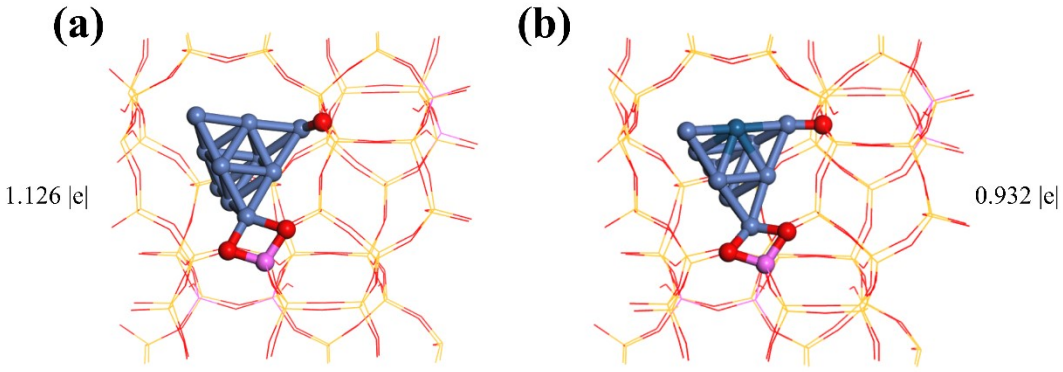

Fig. S28 the optimized structural models of (a) Ni@ZSM-5 and (b) Ni-Pt@ZSM-5.

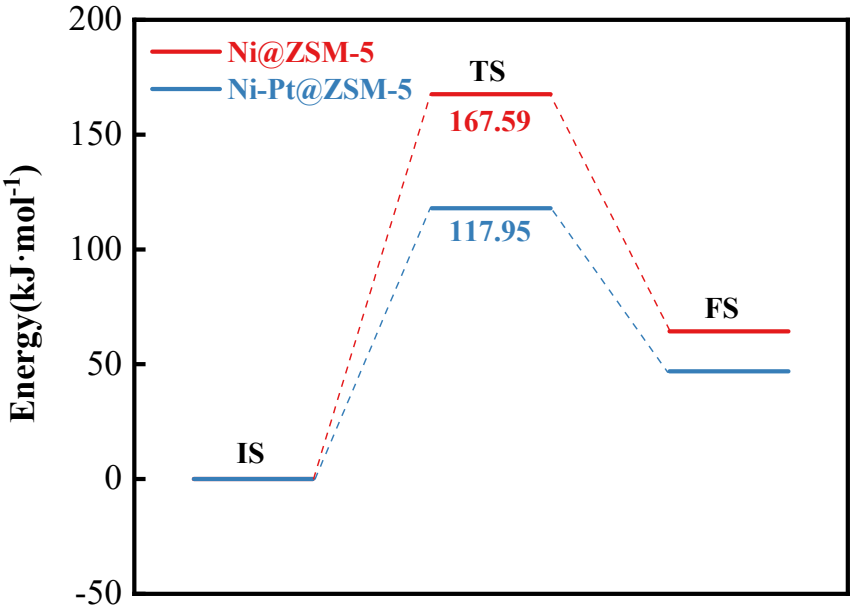

Fig. S29 Methane activation energy of different catalysts.

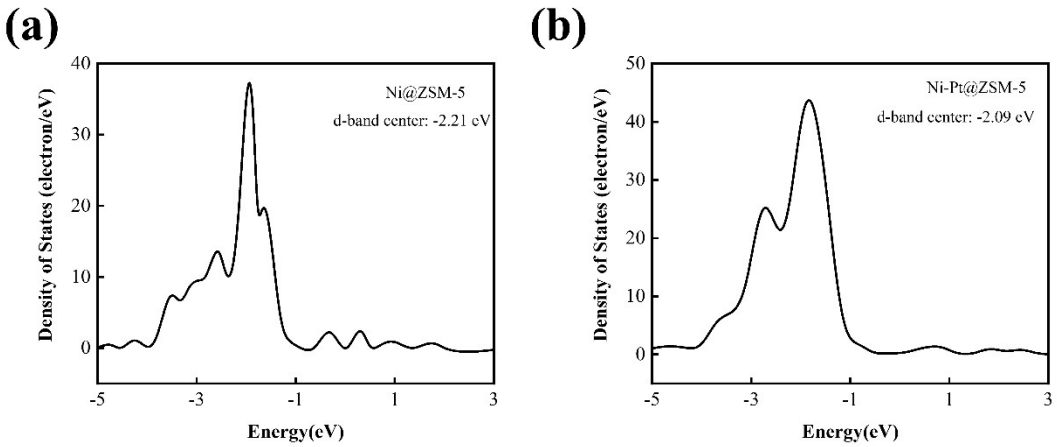

Fig. S30 D-band centers of (a) Ni@ZSM-5 and (b) Ni-Pt@ZSM-5.

Table S1

Metal content and dispersity for the prepared catalysts.

Sample	Pt loading[a](wt%)	Ni loading[a](wt%)	Dispersity[b](%)
Ni-Pt@ZSM-5(25)	0.43	0.96	28.6
Ni-Pt@ZSM-5(50)	0.37	0.98	27.9
Ni-Pt@ZSM-5(100)	0.36	1.03	27.5
Ni-Pt@S-1	0.31	1.07	29.3
Ni@ZSM-5(25)	-	1.04	25.6
Pt@ZSM-5(25)	0.32	-	26.2
Ni-Pt/ZSM-5(25)	0.35	1.06	13.2

[a] Measured by ICP-AES.

[b] Analyzed by CO pulse adsorption.

Table S2

Metal content and dispersity for the prepared catalysts.

Sample	Surface area ($m^2 \cdot g^{-1}$)			Pore volume($cm^{-3} \cdot g^{-1}$)		
	Total[a]	Micropore[b]	External[b]	Total[c]	Micropore[b]	Mesopore
Ni-Pt@ZSM-5(25)	408.302	330.486	77.816	0.227	0.139	0.088
Ni-Pt@S-1	410.386	297.879	112.507	0.249	0.136	0.113
Pt@ZSM-5(25)	436.169	365.593	70.576	0.241	0.152	0.089
Ni-Pt/ZSM-5(25)	396.381	243.553	152.828	0.236	0.098	0.138
ZSM-5(25)	420.219	154.511	265.708	0.236	0.106	0.130

[a]Total surface area calculated using BET method.

[b]Micropore surface area, external surface area and micropore pore volume calculated using the adsorbed volume at the relative pressure (P/P_0) of 0.99.

[c]Total pore volume confirmed by t-plot method.

Table S3

Cell parameters of the prepared catalysts

Sample	a/Å	b/Å	c/Å	Å^3
Ni-Pt@S-1	18.6499	19.7512	13.4389	4950.33
Ni@ZSM-5(25)	19.8520	19.7665	13.4054	5260.34
Pt@ZSM-5(25)	19.4653	19.8912	13.3264	5159.82
Ni-Pt/ZSM-5(25)	18.8605	19.7609	13.3682	4982.33
Ni-Pt@ZSM-5(25)	18.8426	19.7811	13.4349	5007.55
Ni-Pt@ZSM-5(50)	18.5378	19.6876	13.4285	4900.93
Ni-Pt@ZSM-5(100)	19.0953	19.7131	13.2405	4984.09
ZSM-5[a]	20.104	19.897	13.395	5358.12

[a]Obtained from the standard PDF card (JCPDS No 40-0003).

Table S4

Results obtained by quantitative NMR analyses

Sample	n_{Si}[a] (mmol/g)	n_{Al}[a] (mmol/g)	n_{Pt}[a] (mmol/g)	n_{Ni}[a] (mmol/g)	$n_{Si(OSi)3(OM)}$[b] (mmol/g)	$n_{Si(OSi)4}$[b] (mmol/g)	$(n_{Si(OSi)3(ONi)}+n_{Si(OSi)3(OPt)})/(n_{Ni}+n_{Pt})$
Ni-Pt@S-1	5.72	0	0.016	0.182	0.603	5.117	3.05
Ni-Pt@ZSM-5(25)	5.76	0.22	0.017	0.180	1.122	4.638	1.23

[a]Analyzed by ICP-AES;

[b]$n_{Si} = n_{Si(OSi)3(OM)} + n_{Si(OSi)4}$; $n_{Si(OSi)3(OM)} = n_{Si(OSi)3(OAl)} + n_{Si(OSi)3(ONi)} + n_{Si(OSi)3(OPt)}$; $n_{Si(OSi)3(OAl)} = 4*n_{Al}$

Table S5. Co-aromatization performance of the as-prepared samples compared with other related catalysts

Catalyst	Reactant	Reaction condition	Methane conversion(%)	Aromatics selectivity(%)	Ref.
Zn/ZSM-5	CH_4+CH_3OH	m(catalysts)=2.0 g; T = 450 °C, molar ratio of CH_3OH to CH_4 = 0.4 ± 0.03,$WHSV_{CH3OH}$ = 1.0 h^{-1}, keep the $WHSV_{CH3OH}$ in CH_3OH feed and CH_3OH cofeed with CH_4 constant, TOS = 20 min	14.8	56.86	[1]
Mo/ZSM-5	CH_4+CH_3OH	T = 700 ℃, P = 0.1 MPa, and GHSV = 2000 mL (CH_4)/(gcat h)	26.4	91.2	[2]
Zn/ZSM-5	CH_4+ phenol	m(catalysts)=1.0 g; m(phenol)=0.1 g; P=2 MPa; T = 400 ℃; Time on stream = 60 min	4.8	62.9	[3]
Ga-Ce-Pt/ZSM-5	CH_4+ oleic acid	m(catalysts) : m(acetic acid)=0.3 :1; P=30bar; T = 400 ℃; Time on stream = 40 min	3.2	50.8	[4]
Zn-Ga/ZSM-5	CH_4+ acetic acid	m(catalysts)=1.0 g; m(acetic acid)=3.0 g; P=0.5 MPa; T = 400 ℃; Time on stream = 40 min	<10%	——	[5]
0.8KPtSn@ MFI	CH_4+C_6H_{14}	Feed (molar ratio): CH_4:N_2 = 18: 5; C_6H_{14}:N_2 = 3:20; CH_4:C_6H_{14}:N_2 = 18:3:2; 271 $WHSV(CH_4)$ = 8 h^{-1} ;$WHSV(C_6H_{14})$ = 7 h^{-1} ; T = 600 ℃; Time on stream = 120 min	7.4	82.0	[6]
Ni-Pt@ZSM-5(25)	CH_4+C_6H_{14}	m(catalysts)=0.2 g; $m(C_6H_{14})$=15 g; P=1.0 MPa; T = 450 ℃; Time on stream = 60 min	10.89	73.40	This work

Table S6 The kinetic data of methane and n-hexane.

Temperature/K	Methane conversion/%	$1/T*10^4K^{-1}$	ln r
673	3.15	14.85884	-12.5528
693	6.19	14.43001	-11.87726
703	6.48	14.22475	-11.83148
713	9.37	14.02525	-11.46269
723	10.89	13.83126	-11.31235

Table S7

Adsorption energy of methane adsorbed on different catalysts.

Model	E_T/Ha	E_{CH4}/Ha	E_{T-CH4}/Ha	Eads/kJ·mol^{-1}
Ni@ZSM-5	-46671.571	-40.457	-46712.104	-199.538
Ni-Pt@ZSM-5	-62501.308	-40.457	-62541.814	-128.650

Table S8

Results of co-reaction of hexene and methane

Temperature (℃)	Reactants	Methane conversion (%)	Selectivity of aromatics (%)
350	C_6H_{12}	0	25.63
	CH_4+C_6H_{12}	1.28	0
400	C_6H_{12}	0	33.28

450	CH_4+C_6H_{12}	3.87	30.28
	C_6H_{12}	0	45.97
	CH_4+C_6H_{12}	5.43	47.42

Reaction conditions：*m*(Catalysts)=0.2 g; *p*＝1.0 MPa; *m*(*n*-hexene)=15 g; *t*=60 min

Table S9

Results of co-reaction of benzene and methane

Temperature (℃)	Methane conversion (%)	Selectivity of toluene (%)	Selectivity of coke (%)
350	0	0	100
400	0	0	100
450	0.13	0.88	99.12

Reaction conditions：*m*(Catalysts)=0.2 g; *p*＝1.0 MPa; *m*(benzene)=15 g; *t*=60 min

References

[1] Z. X. Xi, B. J. Zhou, B. B. Jiang, J. D. Wang, Z. W. Liao, Z. L. Huang, Y. R. Yang, Efficient conversion of methane to aromatics in the presence of methanol at low temperature, Molecular Catalysis, 2019, 475, 110493.
[2] Y. Liu, D. F. Li, T. Y. Wang, Y. Liu, T. Xu, Y. Zhang, Efficient Conversion of Methane to Aromatics by Coupling Methylation Reaction, ACS Catalysis, 2016, 6(8), 5366-5370.
[3] A. Wang, D. Austin, P. He, M. Ha, V. K. Michaelis, L. J. Liu, H. Qian, H. B. Zeng, H. Song, Mechanistic Investigation on Catalytic Deoxygenation of Phenol as a Model Compound of Biocrude Under Methane, ACS Sustainable Chemistry & Engineering, 2019, 7(1), 1512-1523.
[4] J. S. Jarvis, Z. F. Li, S. J. Meng, H. Song, Methane assisted catalyst synthesis and catalytic conversion of oleic acid, Journal of Materials Chemistry A, 2022, 10(36), 18671-18678.
[5] A. G. Wang, D. Austin, A. Karmakar, G. M. Bernard, V. K. Michaelis, M. M. Yung, H. B. Zeng, H. Song, Methane Upgrading of Acetic Acid as a Model Compound for a Biomass-Derived Liquid over a Modified Zeolite Catalyst, ACS Catalysis, 2017, 7(5), 3681-3692.
[6] B. Liu, F. Wang, X. M. Dou, P. F. Li, H. W. Xiang, Y. Yang, P. He, Co-aromatization of methane and hexane over Pt encapsulated in ZSM-5 zeolite and the electronic effect of K promoters, Science China-Chemistry, 2024, 67(3), 1017-1027.